NMR of nuclei near rare-earth ions in yttrium ethyl sulfate*

J. P. Wolfe†
Department of Physics, University of California at Berkeley, Berkeley, California 94720
and Physics Department and Materials Research Laboratory, University of Illinois at Urbana-Champaign, Illinois 61801
(Received 20 December 1976)

Nuclear magnetic resonances are detected for protons adjacent to rare-earth impurities in yttrium ethyl sulfate (YES) crystals at $T < 4.2$ K. The near-proton resonances are shifted several hundred gauss away from the usual bulk proton NMR and are two to four orders of magnitude weaker, depending on the impurity concentration. A sensitive and versatile rf spectrometer used to detect these weak signals is described in detail. The magnitude of the NMR shift is shown to be approximately described by a point dipolar field of the paramagnetic impurity, even for protons only 3 Å from the impurity. However, field-angle dependences of these nearest proton splittings reveal significant deviations from the simple dipolar interaction which most likely arise from the finite extent of the impurity wave function. A frequency dependence of the splitting gives the components of the local field parallel and perpendicular to the external field direction. The intensities of the near-nuclei magnetic resonances (NNMR) in YES:Yb decrease rapidly above 3.8 K. The observed temperature dependence is quantitatively explained for 1.5 K $< T <$ 4.2 K by including time-dependent fluctuations in the local field. A general NNMR criterion is experimentally established: lifetime broadening of the near-nuclei resonances occurs whenever the electron $\langle S_z \rangle(t)$ correlation time τ is shorter than the inverse dipolar NMR linewidth; i.e., when $\tau \lesssim 10^{-5}$ sec for abundant ^{1}H and ^{19}F spins. From the near proton splittings in YES:Yb near $\theta = 90°$, a large distribution in the value of the elusive $g_\perp$ factor was discovered, giving $\tilde{g}_\perp = 0.01$. Comparisons of NNMR spectra for several rare-earth ions in YES and the extension of this method to other crystals are discussed.

I. INTRODUCTION

The interaction between paramagnetic impurities and surrounding nuclear spins in diamagnetic crystals has received much attention over the last decade.[1,2] In most cases studied to date, a transition ion directly replaces a diamagnetic ion in the crystal lattice. Two basic questions that arise for this system are (i) how does the surrounding crystal lattice adjust to the substituted ion, and (ii) what is the electronic wave function of the impurity ion in this crystalline environment? A measurement of the electron-nuclear spin-spin interaction gives basic information concerning both the distortion of the lattice surrounding the paramagnetic ion and the wave function of the unpaired electron spin.

In a few cases, particularly for iron-group impurities, the electron-nuclear interaction is directly reflected in the electron spin resonance (ESR) spectrum with the appearance of resolved superhyperfine structure.[3] A more powerful and general technique, electron-nuclear double resonance (ENDOR), makes use of the fact that the ESR line is inhomogeneously broadened by the local fields of the nearby nuclei. By inducing a radio-frequency transition at precisely the shifted NMR frequency of a particular nearby nucleus, a change in the microwave-saturated ESR signal is often observed. A high-resolution spectrum of radio-frequency transitions is obtained in this way characterizing the electron-nuclear interactions. While not experimentally applicable to all transition ions, the ENDOR technique, invented by Feher in 1956,[4] has been applied successfully to a variety of crystals. Some representative ligand ENDOR experiments are cited in Refs. 5–10.

In this paper, a new and perhaps simpler experimental approach to the problem is described and developed[11]: A high-sensitivity NMR spectrometer is employed to *directly* detect discrete nuclear magnetic resonances of nuclei adjacent the impurity. For the hydrated single crystals considered here, resonances due to the *near protons* on the waters of hydration are shifted away from the *bulk proton* NMR by a local impurity field which may be approximated by a static point-dipolar interaction. It will be shown that the basic criterion for the appearance of sharp well-resolved near-nuclei magnetic resonances (NNMR) is that the impurity moment flip rate $1/\tau$ be slower than the NMR dipolar linewidth $\Delta\omega$, which is about 10^5 sec^{-1} for abundant hydrogen and fluorine spins. This criterion is generally well satisfied for lightly doped transition ions in crystals below 4.2 K.

The quasistatic nature of the local field near dilute paramagnetic impurities produces large temperature-independent splittings of order kilogauss. This situation may by contrasted to previous experiments in which nuclear magnetic resonances are shifted by *time-averaged* local fields. Bloembergen[12] observed the magnetic resonance of protons near Cu^{2+} in $CuSO_4 \cdot 5H_2O$ at low temperatures. The strong exchange interaction between the adja-

cent paramagnetic ions in this *concentrated* crystal caused rapid mutual electron spin flips ($\tau^{-1} \gg \omega$) which resulted in a time-averaged local field. Thus the NMR shifts of the (abundant) nearby nuclei were dependent on the electronic polarization as manifested in strongly temperature-dependent splittings. Shulman and Jaccarino[13] first observed the NMR from abundant ^{19}F nuclei in the antiferromagnetic crystal MnF_2, where the local field is again averaged by electronic spin flips. In metals, Lang, Boyce, Lo, and Slichter[14] first detected the magnetic resonance of ^{63}Cu near Co impurities in copper, where the local field around the magnetic impurity depends upon the conduction-electron spin density. In paramagnetically doped liquid solutions at room temperature, the time-averaged local fields result in milligauss-to-gauss NMR shifts.

The technique described here is widely applicable to single crystals at low temperatures. It is equally applicable to both non-Kramers[15] and Kramers ions and, unlike ENDOR, the relative intensities of the resonances are generally predictable. When compared to the bulk NMR intensity, the near-nuclei magnetic resonance (NNMR) intensities are a direct measure of the impurity concentration. In addition, the sign of the electron-nuclear interaction is readily obtainable even for effective spin-$\frac{1}{2}$ impurities. The basic simplicity of a single NMR spectrometer allows for wide-range frequency dependences (equivalent to an H dependence in ENDOR) and accurate external field-angle dependences[16] necessary for a more complete description of the interactions.

In addition, this NNMR technique is the key to a better understanding of the nuclear relaxation process of spin-$\frac{1}{2}$ nuclei in paramagnetic crystals at low temperatures. The method provides a *microscopic* probe of the relaxation and spin diffusion processes present in a large class of insulating material. Preliminary relaxation experiments for near nuclei have been reported.[11,17] The primary aim of this paper is to explain the *static* NNMR spectrum and its dependence on the externally variable parameters.

The crystals considered here are rare-earth-doped yttrium ethyl sulfate $Y_2(C_2H_5SO_4)_3 \cdot 9H_2O$, abbreviated YES. They have been extensively studied by optical[18] and ESR methods.[1] Trivalent rare-earth ions substitute directly for the diamagnetic Y^{3+}, and the site symmetry is C_{3h}. The local environment of the rare-earth ion is shown in Fig. 1. Nine waters of hydration directly surround the trivalent ion. While the oxygen positions have been determined for pure YES by x-ray analysis,[19,20] the hydrogen positions have previously only been estimated by chemical arguments.[21] In general the orientation of the water molecules directly surrounding the rare-earth ion will be somewhat different from the Y^{3+} site and will also depend upon the particular impurity ion. The NNMR splittings are very sensitive to these small differences.

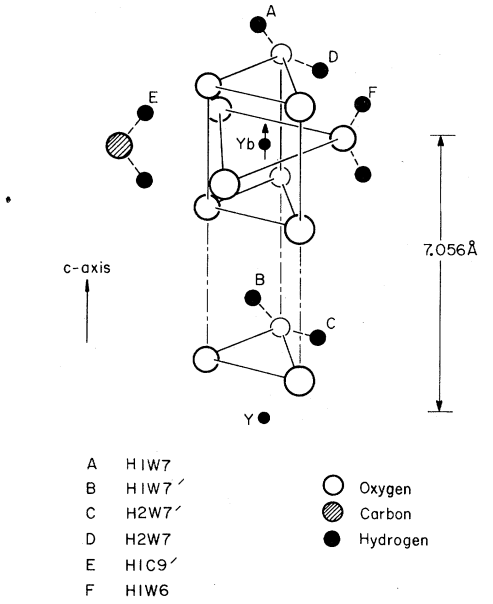

FIG. 1. Local environment of Yb^{3+} in YES. The nine oxygens are located at the vertices of three horizontal equilateral triangles. For brevity in this paper, the crystographic identification for each hydrogen atom has been reduced to a single capital letter. The *B* proton (hydrogen nucleus) is the H1W7 site in the adjacent unit cell.

Trivalent ytterbium ($4f^{13}$, $^2F_{7/2}$ ground multiplet) is a Kramers ion which in YES exhibits an unusually weak ESR signal due to the nature of its ground state. Far-infrared optical measurements of the $^2F_{7/2}$ ground multiplet[22,23] indicated that the $J_z = \pm\frac{3}{2}$ doublet lies lowest, with the next crystal-field doublet at 44 cm^{-1}. More recently, ESR was observed[24] and the measured g factors were found to be $g_{\parallel} = 3.328 \pm 0.005$ and $g_{\perp} \lesssim 0.01$. The small deviation from $g_{\parallel} = 2g_L\langle\frac{3}{2}|J_z|\frac{3}{2}\rangle = 3.429$ for a pure $\pm\frac{3}{2}$ state has been explained as a phonon-induced g shift.[24,25] Because of this large anisotropy in the g factor as well as in the electron spin-lattice relaxation, this crystal has received considerable attention as a proton spin refrigerator.[21,26-29] Unusual and interesting optical pumping effects have also been reported.[30,31] Near-proton resonances were first observed by King for Nd-doped YES; however, the bulk of the experiments to date involve Yb^{3+} due to its unique electron spin-lattice relaxation properties.

Detection of the thermal-equilibrium signal from the few protons near dilute impurities requires a sensitive rf detection scheme, as described herein.

An alternative method is to dynamically polarize the near nuclei by microwave saturation of forbidden ESR, thus enhancing the NNMR signals by two to three orders of magnitude. This method has been used by Hundt, Niebuhr, Derighetti, and Brun[32] to detect ^{27}Al nuclei near Cr^{3+} in ruby. Like ENDOR, this technique requires a microwave spectrometer in addition to the NMR detector, and intensities of the resonances will depend upon the dynamic coupling mechanisms.

Although no ENDOR experiments have yet been reported for YES:R, where R is a rare-earth ion, an extensive ENDOR study has been conducted for a similar hydrated crystal: de Beer[10] investigated the manganese-proton superhyperfine interaction in lanthanum magnesium nitrate doped with Mn^{2+}.

II. INTERACTIONS

The effective spin Hamiltonian for the impurity spin S and a nearby nucleus I in an external magnetic field H is given by

$$\mathcal{H}=\mu_B\vec{S}\cdot\vec{g}\cdot\vec{H}+g_n\mu_B\vec{H}\cdot\vec{I}+\vec{S}\cdot\vec{A}\cdot\vec{I}, \tag{1}$$

which contains electron and nuclear Zeeman interactions and the hyperfine interaction. Here, $\mu_B = 0.927312\times10^{-20}$ erg/G is the Bohr magneton and $g_n = 0.00304$ for protons. Usually the electronic g tensor is known from ESR, and for axially symmetric sites it is simply described by two elements, $g_\parallel$ and $g_\perp$. In general the second-rank hyperfine tensor $\vec{A}=(A_{ij})$ has nine independent elements; however, the symmetry of the impurity site may reduce the number of independent parameters needed to describe $\vec{A}$. If the line connecting S and I is a crystal symmetry axis, then the interaction can be written in a simple dipole-plus scalar form involving only two parameters, A_p and A_s. An example is the nearest-neighbor fluorine at a cubic rare-earth site in CaF_2 which has C_{3v} point symmetry.[2] Unfortunately, for the molecular crystals considered here, no such symmetry exists and a rigorous treatment involves nine independent hyperfine parameters.

Despite this complexity, it will be shown empirically to within a few percent that the hyperfine interaction between the Yb^{3+} ion and even the nearest proton spins in YES can be approximated by the classical point dipolar form

$$\mathcal{H}_d=(1/r^3)[\vec{\mu}_n\cdot\vec{\mu}_e-3(\vec{\mu}_n\cdot\hat{r})(\vec{\mu}_e\cdot\hat{r})]\equiv-\vec{\mu}_n\cdot\vec{h}, \tag{2}$$

where $\vec{r}=r\hat{r}=(x,y,z)=r(\sin\varphi\cos\psi,\sin\varphi\sin\psi,\cos\varphi)$ is the distance from the electronic moment $\vec{\mu}_e$ to the nuclear moment $\vec{\mu}_n=g_n\mu_B\vec{I}$ in terms of the crystalline axes with $\vec{z}\|\vec{c}$. Figure 2 illustrates the local field and the coordinate axes chosen. In this paper, it is assumed as a first approximation that $\vec{\mu}_e$ is fixed at the position of the impurity nucleus. Corrections to this simplified interaction due to the finite extent of the impurity wave function will no doubt become more apparent as angle-dependent NNMR splittings for several rare-earth ions in YES are obtained.

Even with this simplified interaction, the calculation of the near-proton splittings is complicated by the fact that the electronic Zeeman interaction is highly anisotropic. For a general field angle, neither the electronic nor nuclear moments are quantized along the external field.

For an external field $\vec{H}=(H\sin\theta,0,H\cos\theta)$ in the xz plane, the electronic moment is quantized along a z' axis. The electronic Zeeman interaction may be written

$$\begin{aligned}\mathcal{H}_{eZ}&=\mu_B(\vec{S}\cdot\vec{g}\cdot\vec{H})\\&=\mu_B(g_\perp H\sin\theta\,S_x+g_\parallel H\cos\theta\,S_z)\\&=g\mu_B\cdot S_z'H.\end{aligned} \tag{3}$$

The appropriate transformations are $S_z'=aS_z+bS_x$, $S_x'=-bS_z+aS_x$, and $S_z=aS_z'-bS_x'$, $S_x=bS_z'+aS_x'$ with $a=(g_\parallel/g)\cos\theta$, $b=(g_\perp/g)\sin\theta$ and $g^2=g_\parallel^2\cos^2\theta+g_\perp^2\sin^2\theta$. The electronic moment $\vec{\mu}_e\equiv(\mu_x,\mu_y,\mu_z)$ may be written

$$\begin{aligned}\vec{\mu}_e&=\langle-\mu_B\vec{g}\cdot\vec{S}\rangle\\&=-\mu_B(\langle S_x\rangle g_\perp,\langle S_y\rangle g_\perp,\langle S_z\rangle g_\parallel)\\&=-\mu_B\langle S_z'\rangle g^{-1}(g_\perp^2\sin\theta,0,g_\parallel^2\cos\theta),\end{aligned} \tag{4}$$

with $\langle S_z'\rangle$ the expectation value of S_z', and $\langle S_x'\rangle=\langle S_y'\rangle=0$. Therefore, the local impurity field at the nucleus located at $\vec{r}=(x,y,z)$ is

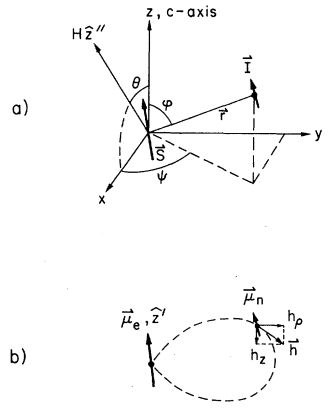

FIG. 2. (a) Coordinate axes for the electron-nuclear system. The external field $\vec{H}=H\hat{z}''$ is defined to be in the xz plane. Due to the electronic g-factor anisotropy, $\vec{\mu}_e$ is quantized along an axis z' as derived in the text. (b) Local field $\vec{h}$ produced at the nucleus due to the electronic moment $\vec{\mu}_e$.

$$\vec{h} = -(1/r^3)[\vec{\mu}_e - 3(\vec{\mu}_e \cdot \hat{r})\hat{r}]$$
$$= (1/r^5)\{[\mu_x(3x^2 - r^2) + 3\mu_z xz]\hat{x} + 3(\mu_z zy + \mu_x xy)\hat{y} + [\mu_z(3z^2 - r^2) + 3\mu_x xz]\hat{z}\}, \quad (5)$$

with μ_x, μ_y, μ_z given by Eq. (4). The total field at the nucleus is the vector sum of this impurity field and the externally applied field

$$\vec{H}_{tot} = \vec{H} + \vec{h}. \quad (6)$$

Since the nuclear moment is isotropic, the nuclear-magnetic-resonance condition is

$$h\nu_0 = g_n\mu_B |\vec{H}_{tot}| = g_n\mu_B(H^2 + h^2 + 2\vec{h}\cdot\vec{H})^{1/2}.$$

Solving for the externally applied field required for resonance, one obtains

$$H = [H_0^2 - h^2 + (\vec{h}\cdot\hat{z}'')^2]^{1/2} - \vec{h}\cdot\hat{z}'', \quad (7)$$

where $\hat{z}'' = (\sin\theta, 0, \cos\theta)$ is the unit vector along the external field, and $H_0 = \hbar\omega_0/g_n\mu_B$ the bulk NMR field. In general, for a given nuclear site and field angle, there are $2S+1$ resonances, corresponding to the various orientations $\langle S_z' \rangle$ of the impurity spin. For the ions considered here, $S = \frac{1}{2}$, and throughout this paper the two resonances corresponding to $\langle S_z' \rangle = \pm\frac{1}{2}$ will be referred to simply as $S_z = \pm\frac{1}{2}$ with $S_z = -\frac{1}{2}$ the lowest electronic level.

For the particular case where H is parallel to the crystal c axis ($\theta = 0, H = H_z$), Eq. (7) simplifies to

$$H = (H_0^2 - h_\rho^2)^{1/2} - h_z, \quad (8)$$

with

$$h_z = -(g_{\parallel}\mu_B/r^3)\langle 2S_z' \rangle(3\cos^2\varphi - 1), \quad (9)$$

$$h_\rho = -(g_{\parallel}\mu_B/r^3)\langle 2S_z' \rangle(3\cos\varphi\sin\varphi), \quad (10)$$

the components of the local field parallel and perpendicular to H. For $H \gg h_\rho, h_z$ the near-proton splitting is approximately $-h_z$. This is because the nuclear spin is quantized nearly along the large external field. The quadratic contribution of h_ρ arises because the nuclear-quantization axis is actually along the total field $\vec{H} + \vec{h}$.

III. APPARATUS AND CRYSTALS

In these experiments it is important that the paramagnetic ions in the crystal are well separated. The reasons are twofold: (i) mutual spin flips between impurities contribute to the local-field fluctuations at nearby nuclei (i.e., they increase τ^{-1}) and (ii) for high-impurity concentrations the resonances of nuclei near one paramagnetic ion are broadened by the fields of the other randomly located ions. To avoid these sources of linewidth broadening the impurity concentration must be less than 10^{-2} to 10^{-5} depending upon the particular ion and type of crystal. Thus a high-sensitivity spectrometer is needed to detect the small number of nuclei near the lightly doped impurities.

A broadband bridge scheme, shown in Fig. 3, has been developed for both high sensitivity and versa-

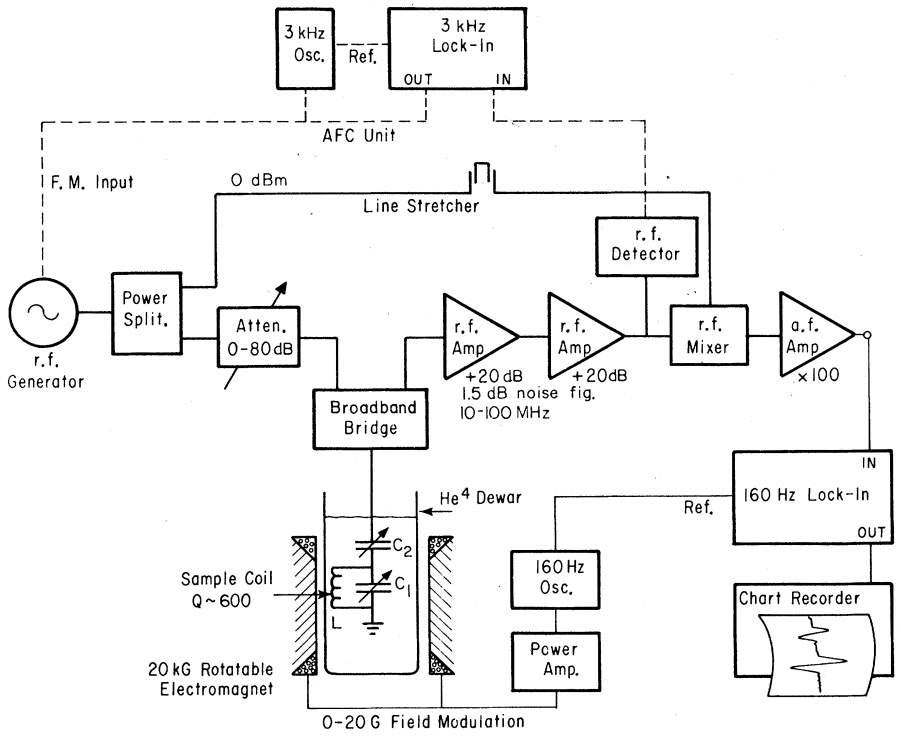

FIG. 3. NMR spectrometer used in these experiments. The sample is placed in a high-Q LC circuit whose impedance is transformed to 50 Ω directly in the helium bath. An rf hybrid tee is used as a bridge to compare the resonant circuit to 50 Ω. The low-level rf signals from the bridge are amplified and then detected by an rf phase-sensitive detector. An automatic-frequency-control (afc) circuit minimizes noise resulting from drifts in the rf generator and the LC circuit.

TABLE I. Radiofrequency components used in the NMR spectrometer.

Component	Manufacturer	Model
rf generator	Marconi	TF1060B/LR
attenuators	Wavetek	5010, 5070
power splitters	Relcom	H2
bridge (hybrid)	Anzak Electronics	H-81
amplifiers	Avantek	UA-142
	Radiation Devices	BBA-1PB
mixer	Relcom	M1C
phase shifter	General Radio	874-LTL

tility.[33] In a given experiment the radio frequency ν_0 is fixed between 20 and 80 MHz while the external magnetic field (0–20 kG) is swept slowly through the resonant NMR fields. A conventional 160 Hz field modulation and lock-in detection is employed. Use of broadband amplifiers (10–100 MHz) with rf phase-sensitive detection gives an effective rf bandwidth equal to the audio bandwidth (10 kHz). Adjustment of ν_0 over a factor of 3 is possible throughout the course of a single run while retaining the low noise characteristics of a tuned receiver. Our experiments have employed both rf components fabricated in this laboratory[33] and commercially available units with comparable results. Table I lists some typical rf components which were used.

A unique feature of this system is the high Q of the resonant circuit. The sample coil is wound directly around the crystal for maximum filling factor and is resonated with capacitor C_1. The coupling capacitor C_2 transforms the impedance of the resonant circuit to 50 Ω *directly* in the helium bath, resulting in a null at the bridge output. The frequency response as observed at the output of the bridge is shown in Fig. 4(b) and corresponds to a loaded $Q \approx 610$. For comparison, a more conventional response, $Q \approx 41$, is obtained when a similar coil (also at 4.2 K) is resonated and matched with room-temperature capacitors. In the latter case the circulating currents of the LC circuit pass through a $\frac{1}{2}\lambda$ cable connecting the coil and the external capacitors, which negates the effect of the lowered coil resistance. In the limit of high Q, the resonance frequency ω_0 is approximately $(LC_1)^{-1/2}$ and the coupling capacitor is given by the relation $C_1/C_2 \approx (QZ_{in}/\omega L)^{1/2}$, with $Z_{in} = 50$ Ω. For a typical four-turn coil (Teflon-coated No. 32 copper wire) and frequency $\nu_0 = 70$ MHz, the values are $L = 0.2$ μH, $C_1 = 20$ pF, and $C_2 \approx 1$ pF. A more-detailed analysis of this circuit reveals that the NMR sensitivity is proportional to Q for a constant rf input level and $Q^{1/2}$ under the condition of constant NMR flip-rate $w_{rf} \sim (g_n \mu_B H_1)^2/\hbar^2$.

The bridge acts to cancel noise from the rf generator while comparing the probe impedance to 50 Ω; for rf input levels up to about −10 dBm (10^{-4} W) the major sources of noise are the rf preamp and thermal noise in the bridge and coil. A crossed coil arrangement has also been used in place of the bridge, and at rf input levels below about −30 dBm, an expected factor of 2 in sensitivity is gained for a given ω_{rf}. At higher levels, rf generator noise is dominant due to the difficulty of making the coils precisely orthogonal in the helium bath. A distinct advantage of the crossed coil arrangement is that the output noise is limited only by the the first rf preamp, since the thermal noise of the resonant coil is negligible at 4.2 K. Nevertheless, the bridge arrangement of Fig. 1 is more frequently used since nuclear-relaxation experiments often employ the second crossed coil for simultaneous excitation at frequencies other than ν_0. For both bridge and crossed-coil schemes, the rf input is generally adjusted below the level at which the near-nuclei resonances are saturated. For example, the rf input to the bridge in Fig. 6(c) is −50 dBm corresponding to $w_{rf} \approx 10^{-4}$ sec^{-1} at 70 MHz.

With the high Q's reported here, the system noise and sensitivity is affected by small frequency shifts in either the LC resonance or the rf generator. It was often found helpful to lock the source frequency onto the sample coil resonance using an automatic frequency control scheme, Fig. 3, similar to those used in ESR spectrometers.[34] A small amount of 3-kHz modulation is applied to the FM signal generator which results in a 3-kHz amplitude modulation of the rf level after the bridge (Fig. 4). This modulation is detected and its phase compared to a 3-kHz reference to provide the correction voltage for the rf generator.

The sample is mounted on a specially designed crystal rotator, Fig. 5, which allows precise and reproducible angular variations to better than 0.1° accuracy. The variable plunger capacitors C_1 and

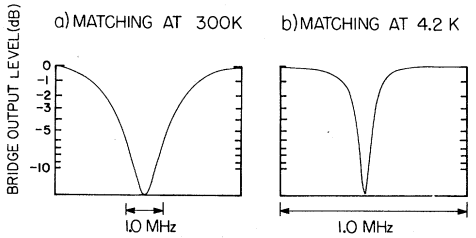

FIG. 4. Frequency response curves of the resonant circuit. The detected output of the bridge is recorded as the rf frequency is swept slowly through $\nu_0 \approx 70$ MHz. (a) Capacitors C_1 and C_2 are external to the bath resulting in a conventional response with $Q \approx 41$. (b) C_1 and C_2 are located directly in the helium bath resulting in high Q. This is the standard configuration in the experiments.

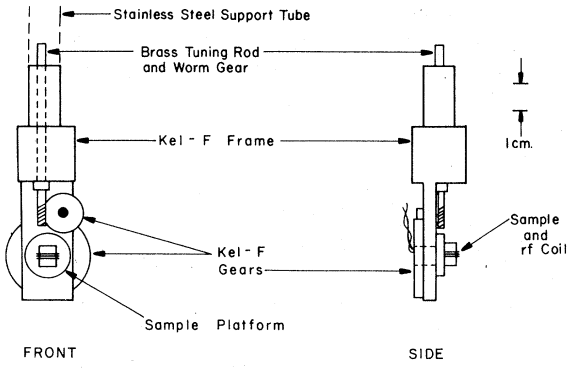

FIG. 5. Crystal rotator for the NMR experiments. For some applications a second rf coil is wound around the plastic pedestal adjacent to the crystal. Usually a 2.5-cm-diam stainless-steel tube is mounted around the entire rotator which acts as a radiation shield.

C_2 are mounted on the Kel-F frame and adjusted by means of stainless-steel tuning rods.

A. Samples

The success of these experiments is based in part upon the large single crystals grown in this laboratory. The crystals were grown with 95.8% enriched ^{174}Yb ($I=0$) and the oxide Y_2O_3 was 99.9999% pure in yttrium. The technique is similar to that used by Stapleton.[35,36] Briefly, the starting chemicals Y_2O_3 (or Yb_2O_3) and $K(C_2H_5SO_4)$ are dissolved in HCl and C_2H_5OH, respectively. The resulting YCl and $K(C_2H_5SO_4)$ solutions are mixed and the KCl precipitated out with a centrifuge. The clear YES-alcohol solution is repetitively vacuum pumped to remove alcohol as H_2O is added. The resulting saturated YES-water solution is placed in a partially covered petri dish in a desiccator at 0°C. Large single YES crystals are formed over a period of several weeks as the water slowly evaporates. The Yb to Y concentrations and masses of the crystals used in the following experiments are listed in Table II.

TABLE II. Weights and concentrations of YES:Yb crystals used in the experiments. The crystal concentration is determined from the integrated NMR intensity of the B resonance compared to the bulk resonance, Eq. (11). S_{bulk}/S_B is the ratio of derivative signal heights at $T \approx 1.6$ K and $\theta = 0$.

Crystal	Yb to Y solution	Yb to Y crystal	Weight (mg)	S_{bulk}/S_B
Yb 1	5%	1.1%	630	145
Yb 2	1.6%	0.4%	964	270
Yb 3	0.5%	0.12%	830	1100
Yb 4	0.2%	0.06%	465	1840

IV. NEAR-PROTON SPECTRUM FOR YES: Yb

A. General observations

Figure 6 shows the near-proton NMR spectrum for crystal Yb 1 when the external field H is carefully aligned along the crystal c axis. ($\theta < 0.1°$.) Figure 6(a) is the ordinary bulk-proton resonance displaying a common Pake structure due to the pure nuclear-nuclear interactions.[37] As the spectrometer gain is increased, discrete resonances are detected up to 500 G away from the bulk resonance. The six outermost resonances are assigned the letters A through F which identifies them with the particular proton sites of Fig. 1, as determined from the following analysis. Lines A through D are sixfold degenerate when $\vec{H} \| \vec{C}$, due to the C_{3h} symmetry of the site. (This degeneracy is displayed for line A in YES: Tb^{3+}, Fig. 18.)

The initial identification of these lines proceeded naturally with the assumption of a pure point dipole interaction, using the estimated proton positions of McColl based on the x-ray results, and with $g_{\parallel} = 3.328$ measured by ESR. Thus, the midplane water protons F at an estimated $r = 3.2$ Å from the ion were predicted to resonate at 384 G above the bulk NMR for $S_z = -\frac{1}{2}$. This corresponds convincingly to the high field doublet, whose midpoint is shifted 390 G from the bulk. This observation provides a

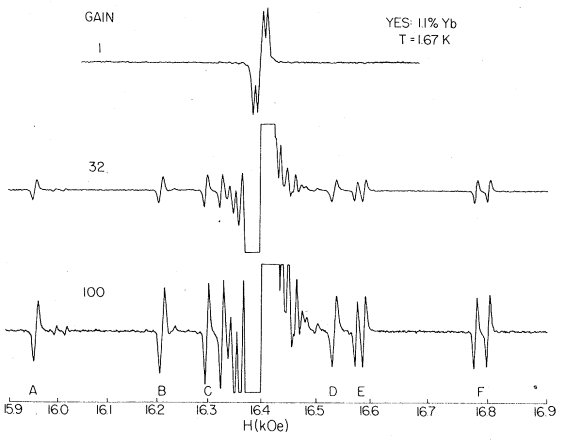

FIG. 6. NMR of protons in sample Yb 1. Trace (a) shows the usual bulk resonance at $H_0 = 16.4$ kOe corresponding to proton spins far from any impurity. As the gain is incr ased in traces (b) and (c) a number of weaker resonances appear due to protons near the Yb^{3+} ion. The external field is accurately aligned along the crystal c axis ($\theta = 0$). The resonances A through F correspond to the proton sites in Fig. 1. The rf input to the bridge in trace c is -50 dBm, the total sweep took approximately 5 min with an output time constant of 0.3 sec. Field modulation was 5 G and NMR frequency $\nu_0 = 69.8$ MHz.

clear indication that the scalar or covalent interaction for these very near protons is much smaller than the dipolar interaction and that the point-dipolar interaction is a reasonable first approximation.

The doublet nature of this resonance (F) arises from the nuclear dipole-dipole interaction between the two equivalent protons on the same water molecule.[37] The measured splitting of 22.3 ± 0.5 G corresponds to a proton-proton distance of 1.56 ± 0.01 Å, to be compared with the H_2O gaseous phase separation[38] of 1.514 Å. With $\vec{H} \| \vec{c}$, the resonances A and D are simply broadened by this nuclear dipole-dipole interaction, and at larger field angles the angular-dependent nuclear-dipolar interaction results in a resolved Pake structure for these resonances also. A plot of this Pake splitting versus field angle, while not analyzed in detail in this paper, contains information about the relative spatial positions of these protons.[10]

Identification of the lowest field resonance with site A is also unambiguous; however, the predicted splitting of −355 G is considerably different from the measured splitting of −445 G. This is because the previously estimated positions of protons A and D were much less certain than that of proton F, whose position is constrained by the reflection symmetry.

The resonance from the D site is not greatly shifted from the bulk resonance because $h_z \sim 3\cos^2\varphi - 1$ is small for this site. The predicted splitting is −86 G using McColl's positions. Experimental identification of the D proton resonance required measurements of the quadratic NMR shifts with frequency, as described in Sec. IV C; it is actually found to lie +135 G above the bulk for $\nu_0 = 70$ MHz. The measured splittings of A and D resonances are explained by a small reorientation of the water molecule from the previous estimates. These proton positions will be determined in Sec. IV C. The fact that the A and D protons belong to the same water molecules and yet give rise to resonances 600 G apart emphasizes the sensitivity of the NNMR splittings to the precise proton positions.

Since the impurity electron moment (effective spin-$\frac{1}{2}$) can occur in either $S_z = -\frac{1}{2}$ or $+\frac{1}{2}$ states, one expects to observe two distinct resonances for each proton site. ($S_z = -\frac{1}{2}$ defines the lowest electronic energy state.) In most cases, the $S_z = -\frac{1}{2}$ line is more intense than the $S_z = +\frac{1}{2}$ line simply by the electronic Boltzmann factor $\exp(g\mu_B H/kT)$, which equals 9.0 at $H = 16.4$ kOe and $T = 1.67$ K of Fig. 6(c). The ability to distinguish $S_z = +\frac{1}{2}$ and $-\frac{1}{2}$ components immediately defines the sense of the local field and hence the sign of the hyperfine interaction.[39] In Fig. 6(c), the $S_z = +\frac{1}{2}$ resonance of proton F lies at 16.01 kOe with approximately 10% of the intensity of the $S_z = -\frac{1}{2}$ lines. The $S_z = +\frac{1}{2}$ and $-\frac{1}{2}$ lines are not completely symmetric about the bulk resonance because of the quadratic shift, Eq. (8), discussed in Sec. IV C. It is convenient, nevertheless, to refer to the $S_z = -\frac{1}{2}$ and $S_z = +\frac{1}{2}$ as the "principal" and "mirror" components, respectively. The mirror resonance of proton A is obscured by the principal F lines at 16.8 kOe.

The intensities of the near-proton resonances are related in a direct way to the actual concentration of impurities in the sample. For low enough concentrations, the derivative signals heights are simply proportional to the concentration; however, at higher actual concentrations (above 1% Yb) the NNMR lines are broadened as previously discussed. In either case an accurate measure of the impurity concentration requires a comparison of the total integrated intensity of an NNMR line with the total integrated intensity of the bulk resonance. For this reason a simple integrating circuit utilizing two IC's was constructed to record the first and second integrals of the derivative NMR line, as shown in Fig. 7. The integrated signals have lower noise levels due to the increased effective time constant. Note that both line A and lines F represent six near protons, although the peak-to-peak derivative signal height S_A is less than $2S_F$ due to the unresolved structure in A. The total integrated intensities I_A and I_F, however, are the same within the accuracy of the measurement or about 20%, Fig. 7(c). In YES,

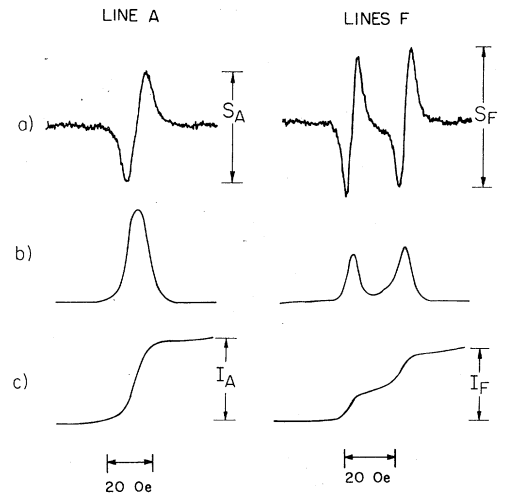

FIG. 7. (a) Derivative traces of the A and F resonances. (b) and (c) first and second integrals of the derivative signals are obtained in successive field sweeps. The F resonance was slightly saturated in this experiment by the rf field, thus the total integrated intensities I_A and I_F are not precisely equal.

where the number of protons per half unit cell is 33, the rare-earth concentration is given by

$$c = \tfrac{11}{2}(I_A + I_{A'})/I_{\text{bulk}}. \quad (11)$$

When the electronic polarization departs significantly from unity, the intensity of the mirror resonance $I_{A'}$ must be included in Eq. (11). Care must be exercised to avoid saturation of the resonances and to account for even small differences in the field sweep rate from one line to the next. The measured Yb concentrations of Table II were obtained by this method.

B. Intensities and linewidths of the near-proton resonances

In the early stages of these experiments, it was observed that the derivative signal heights [Fig. 7(a)] of the near-proton lines for YES:Yb are diminished by over an order of magnitude as the temperature is raised to 4.2 K. The key to this phenomenon lies in the fact that the local impurity field at a given near nucleus is not completely static. Indeed, the sense of the local field is reversed when the impurity moment flips via electron spin-lattice relaxation (SLR) or mutual spin flips with nearby impurities. It will be shown here that rapid electron spin-lattice relaxation at 4.2 K causes a broadening of the NNMR linewidths ΔH and a corresponding decrease in the peak-to-peak derivative signal height S. The reason for a decrease in S is that for a constant number of nuclear spins with a given spin polarization and a constant NMR line shape the total integrated intensity, $I \sim S(\Delta H)^2$, is conserved. A quantitative description of this effect is given below. The calculation gives a basic criterion for observation of the NNMR spectrum.

The Yb^{3+} ion in YES is a particularly good probe of this phenomenon since its electron SLR rate can be varied over six orders of magnitude by merely adjusting the temperature of the crystal between 1.6 and 4.2 K, as shown in Fig. 10(b). The electron SLR rate at $\theta = 0$ is approximately given by

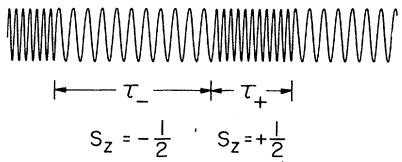

FIG. 8. Schematic showing the source of the NNMR linewidth broadening at higher temperatures. The nuclear Larmor frequency of a near-proton depends on the external-plus-local field, which switches from $H_0 - h_z$ to $H_0 + h_z$ as the electron spin flips between $S_z = \pm\frac{1}{2}$. The average times τ_+ and τ_- depend on the electron-spin lattice relaxation time and the electronic Boltzmann factor. The nuclear precession frequencies are less well defined at high temperatures where $\tau_\pm$ are short.

$$T_{1e}^{-1} = 0.0135T^9 + 5.1\times 10^{11}\exp(-59/T), \quad (12)$$

where the T^9 Raman coefficient was measured[24] for YES:Yb and the Orbach term was determined[40] for pure YbES.

The situation is illustrated schematically in Fig. 8. Here the nuclear Larmor precession of a near nucleus depends upon the S_z of the rare-earth ion and the external field H. For thermal equilibrium, the average lifetime of the $S_z = +\frac{1}{2}$ and $-\frac{1}{2}$ states are denoted by τ_+ and τ_-, and the ratio τ_+/τ_- equals the Boltzmann factor. The spin-lattice relaxation rate is $T_{1e}^{-1} = \tau_+^{-1} + \tau_-^{-1}$. The spectral distribution of the nuclear magnetization, $M_x \sin\omega_0 t$, beginning at $t = 0$ and ending at $t = \tau$ is given by the Fourier transform

$$f(\omega,\tau) = \int_0^\tau \sin\omega t \sin\omega_0 t\, dt = \frac{1}{2}\frac{\sin(\omega-\omega_0)\tau}{\omega-\omega_0}. \quad (13)$$

For a random process with probability $P(\tau) = \tau_0^{-1}\exp(-\tau/\tau_0)$ of a spin flip at time τ, the time-averaged spectral distribution is

$$F(\omega) = \int_0^\infty P(\tau) f(\omega,\tau)\, d\tau = \frac{1}{2}\frac{\tau_0}{1+(\omega-\omega_0)^2\tau_0^2}, \quad (14)$$

which is a Lorentzian line shape. Substituting $\omega = g_n\mu_\beta H/\hbar$ and $\tau_0 = \tau_\pm$, the peak-to-peak derivative linewidth of $F(H)$ for the $S_z = \pm\frac{1}{2}$ lines is

$$\Delta H_\pm = \frac{2}{\sqrt{3}}\frac{\hbar}{g_n\mu_B}\frac{1}{\tau_\pm}. \quad (15)$$

The lifetimes $\tau_\pm$ are expressed in terms of the electron SLR rate and the Boltzmann ratio by

$$\tau_- = T_{1e}(1+\delta_-) \equiv T_{1e}\gamma_- \quad (16a)$$

and

$$\tau_+ = T_{1e}(1+\delta_+)/\delta_+ \equiv T_{1e}\gamma_+, \quad (16b)$$

where $\delta_\pm = \exp(g_e\mu_B H_\pm/kT)$, and $H_\pm$ are the resonant fields of the $S_z = \pm\frac{1}{2}$ NNMR lines. Note that $\delta_+ \approx \delta_-$ within 4% for these high-field experiments. Thus, the Lorentzian contribution to the near-proton linewidth by this process is found to be

$$\Delta H_\pm = (4.32\times 10^{-5}\ \text{G sec})\, T_{1e}^{-1}\gamma_\pm^{-1}. \quad (17)$$

For YES:Yb, this contribution becomes observable above 3.5 K, where T_{1e}^{-1} is large. Figures 9(a) and (b) are derivative tracings of the F lines at 1.7 and 4.2 K, respectively. The lines are considerably broader at 4.2 K and display long Lorentzian tails characteristic of this T_{1e} broadening mechanisms. At temperatures below 3.5 K the NNMR linewidth is predominantly[41] due to nuclear dipole-dipole interactions, and is denoted by ΔH_0.

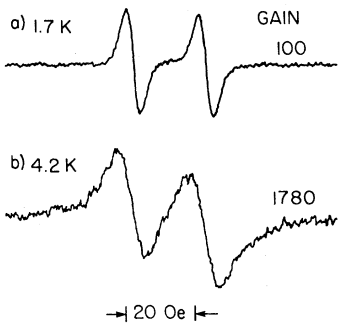

FIG. 9. Traces of the F resonances for (a) $T=1.7$ and (b) $T=4.2$ K. The peak-to-peak derivative height at 4.2 K is $\sim 17\times$ smaller than at 1.7 K due to the linewidth broadening by rapid fluctuations in the local field. Long Lorentzian tails characteristic of lifetime broadening are readily observed in the high-temperature data.

As expected, the low-temperature line shape is much closer to Gaussian than Lorentzian. For example, line A in Fig. 7(b) displays an almost perfect Gaussian line shape.

Due to the above broadening mechanisms, the signal height of the near-proton resonance is probably most accurately given in terms of a convoluted Voigt line shape,[42] which cannot be simply expressed in closed analytic form. However, it is reasonable to approximate the total integrated intensity by the simple analytic form

$$I_{\pm} = S(\Delta H_0^2 + K\Delta H_{\pm}^2)\,, \tag{18}$$

where the change in line shape is incorporated into the parameter K. If ΔH_0 and ΔH_+ are the peak-to-peak derivative linewidths for pure Gaussian and pure Lorentzian lines, then the total integrated intensity is conserved in these two limits when[42] $K=3.51$. The total integrated intensity I of a near-proton resonance is proportional to the nuclear polarization, $p_n=\tanh(g_n\mu_B H_{\pm}/2kT) \approx g_n\mu_B H_{\pm}/2kT$, and the fractional population $f_{\pm}$ of the corresponding electronic state. The derivative signal height may then be written

$$S = C(g_n\mu_B H_{\pm}/2kT)f_{\pm}/(\Delta H_0^2 + K\Delta H_{\pm}^2)\,, \tag{19}$$

where the constant C depends on the impurity concentration as well as the sensitivity of the spectrometer.

The peak-to-peak derivative signal heights for both $S_z=\pm\frac{1}{2}$ F lines are plotted versus temperature in Fig. 10(a). The dotted curves represent $(H_{\pm}/T)f_{\pm}$, which would be the intensity if there were no lifetime broadening ($\Delta H_{\pm}=0$). The solid curves are a simultaneous fit of all the measured intensities (including both $S_z=\pm\frac{1}{2}$) to Eq. (19), allowing only K and C to vary. For the Orbach rate given above, and the measured $\Delta H_0=5.0$ G, these curves correspond to $K=5.20$. Alternatively, by setting $K=3.51$ and using the more recently measured splitting of 63 °K for the first excited doublet, the Orbach SLR rate is determined to be $(1.6\pm0.3)\times10^{12}\exp(-63/T)$ from a least-squares fit to the NNMR intensities. At 4.0 K this expression predicts a rate only 15% higher than Eq. (12); which is within the stated error of the Dutch SLR results. The above analysis, therefore, seems to provide a good quantitative explanation of the observed NNMR intensities over the liquid-helium temperature range. The Orbach rate, as expected, is close to that obtained for pure YbES.

From Fig. 10 and Eqs. (17) and (19) is readily deduced that the signals are diminished by a factor of 2 when $\tau_{\pm}^{-1}=2\times10^5\ \mathrm{sec}^{-1}$. This implies a general near-nuclei magnetic resonance criterion. The NNMR resonances will be broadened by the fluctuating local field unless

$$\Delta\omega_0\tau_{\pm} \geq 0.67\,, \tag{20}$$

where $\Delta\omega_0=\gamma\Delta H_0$, which for protons becomes

$$\tau_{\pm} \geq 2.5\times10^{-5}\ \mathrm{G\,sec}/\Delta H_0\,. \tag{21}$$

It is interesting that this criterion is independent

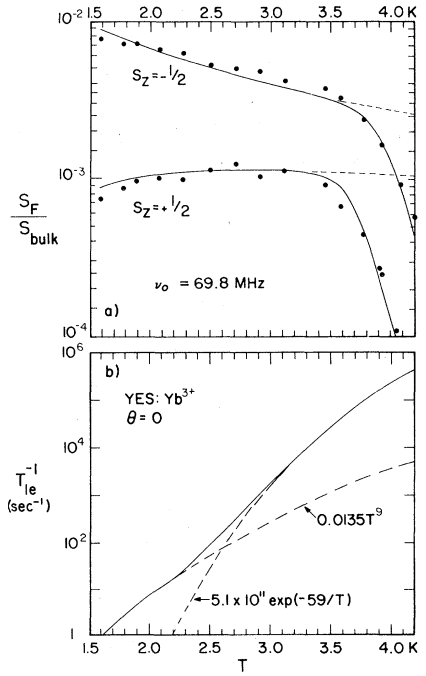

FIG. 10. (a) Temperature dependence of the peak-to-peak derivative NNMR intensity for proton F. (Crystal Yb 1.) Nearly identical data are obtained for the other resolved resonances of Fig. 6(c). The rapid decrease in intensity above 3.8 K is due to electronic spin-lattice relaxation. (b) Note that the NNMR signals are reduced by a factor of 2 when $T_{1e}^{-1}\approx2\times10^5\ \mathrm{sec}^{-1}$. The electron relaxation rate is from Eq. (12).

of the NNMR splitting.[43] This has been experimentally verified: The temperature dependence of the signal heights for all of the other resolved lines of Fig. 6(c) was also observed. With correction for small differences in ΔH_0, the results are essentially the same as for the $S_z = -\frac{1}{2}$ resonance in Fig. 10(a).

In general mutual spin flips between impurities will also contribute to $\tau_\pm$. The calculation of the mutual flip rate of two Yb^{3+} ions as a function of Yb concentration is complicated by the presumed random arrangement of the paramagnetic ions. For a simple cubic lattice with minimum spacing, a, between ions and isotropic $S = \frac{1}{2}$ electron spins, Buishvili *et al.*[44] determined the S_z correlation time due to spin-spin interactions to be

$$T_{2e}^{-1} = \alpha c g_e^2 \mu_B / \hbar a^3 , \tag{22}$$

where $\alpha = \frac{2}{3}$ for a random concentration c of impurity ions. For YES:Yb^{3+}, the g factor must be replaced with $g_e = g_\perp \lesssim 0.01$, and $a^3 \approx 1200$ Å^3, giving the approximate result $T_{2e}^{-1} \approx 45$ sec^{-1} for $c = 0.01$. Thus from Eq. (20) mutual electronic spin flips will have a negligible influence on the NNMR linewidth, $\Delta\omega \approx 10^5$ sec^{-1}. In general, however, this can be an important mechanism which sets an upper limit to the usable impurity concentration. For example, if $g_e = 2$ and $a = 3.43$ Å as for the CaF_2 crystal, then setting $\tau_\pm = T_{2e}$ and using Eqs. (21) and (22) leads to the requirement $c \lesssim 4 \times 10^{-5}$ for the observation of "unbroadened" near-fluorine resonances. Our investigations of the CaF_2:R system indeed indicate that additional broadening of the near ^{19}F resonances is prevalent for actual concentrations greater than 10^{-4}. This means that one must be able to detect near-fluorine intensities 10^4 to 10^5 times smaller than the bulk resonances. Detection of these resonances generally requires rf input power levels 100 to 1000 times those used in the present experiment for increased sensitivity. In some cases this results in a partial rf saturation of the resonances, depending on the near-fluorine relaxation times.

The opposite limit to this situation is illustrated by Bloembergen's experiment[12] on copper sulfate where the local field is fluctuating so rapidly ($\tau^{-1} \gg \omega$) that the NMR is again narrowed. Between these two limits of high and low paramagnetic concentrations, the NNMR resonances are washed out by the local field fluctuations.

Thus one concludes that as T_{1e}^{-1} is increased, the broadened near-nucleus line will eventually shift towards the bulk resonance. In the extreme limit the $S_z = \pm\frac{1}{2}$ will presumably form a single resonance corresponding to the time-averaged local field. A small shift of order 2 G towards H_0 was observed for the A and F resonances as the temperature was increased to 4.2 K, where $T_{1e} \approx 2.5 \times 10^{-6}$ sec. This fact underscores the difference between impurity shifted NMR lines in dilute low temperature solids and the local NMR in metals, liquid solutions, and concentrated solids. In the latter cases $\tau^{-1} > \omega$ and the local fields are time averaged; thus, the splittings are dependent on the electronic polarization, p_e. In dilute paramagnetic solids below 4.2 K, usually $T_{1e}^{-1} < \Delta\omega$ and the local fields are relatively static: the NMR splittings are independent of T_{1e} and p_e.

C. Frequency dependence of the spectrum

The resonant condition, Eq. (8), implies that the splitting $H - H_0$ depends upon H_0, and therefore upon the rf frequency $\nu_0 = g_n \mu_B H_0 / h$. Since h_ρ^2 is quadratic in S_z, the shift $(H_0^2 - h_\rho^2)^{1/2} - H_0$ is the same for both $S_z = \pm\frac{1}{2}$ and will be towards lower fields for both principal and mirror resonances. Physically the quadratic shift comes about because the axis of spin quantization of the near nucleus is not directly along the externally applied field. An important consequence is that for a given field angle the local-field components, h_z and h_ρ, may be independently determined by varying the frequency. A knowledge of these components is particularly useful for predicting the nuclear relaxation rate of individual near nuclei, where fluctuations in the radial component $h_\rho(t)$ are the source of direct relaxation to the impurity. Also, in cases where the impurity field is largely point dipolar, h_ρ and h_z determine the nuclear coordinates (r, φ) with respect to the ion.

For YES:Yb, the measured frequency dependence showed a large quadratic shift corresponding to $h_\rho = 734$ G for the resonance near $H - H_0 = +135$ G, positively identifying this resonance as belonging to the D protons only 3 Å away from the ion [Fig. 11(c)]. In this particular case the h_z component was relatively small due to the large anisotropy of the local field. This assignment was later verified by a field-angle dependence of the splitting.

Figure 11 displays the frequency-dependent shifts of the three nearest proton sites for $20 < \nu_0 < 70$ MHz. As the frequency is decreased both the $S_z = \pm\frac{1}{2}$ lines are shifted equally towards lower fields relative to the bulk resonance, as predicted. The solid curves are least-squares fits to Eq. (8), including both $S_z = \pm\frac{1}{2}$ branches. The resulting local-field components are given in Table III.

The coordinates of these nearest protons are obtained by inverting the Eqs. (9) and (10) for a point dipolar interaction, which gives

$$\cos\varphi = \left(\frac{R + 6 \pm (R^2 + 8R)^{1/2}}{2(R+9)} \right)^{1/2} \tag{23}$$

and

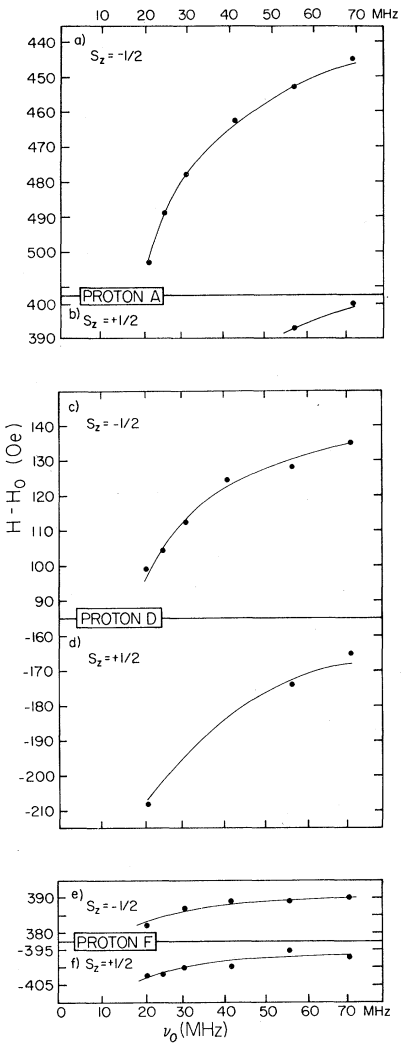

FIG. 11. Frequency dependence of the NNMR splittings for A, D and F protons. Solid lines are least-squares fits to Eq. (8) giving the local-field components listed in Table III.

$$r = \left(\frac{g_{\parallel} \mu_B (3\cos^2\varphi - 1)}{h_z} \right)^{1/3}, \tag{24}$$

where $R = (3h_z/h_\rho)^2$ and the adjustable sign in the first equation equals the sign of h_z. The resulting values of r and φ are also given in Table III. The radii obtained by this method for protons A, D and F are close to those predicted previously: 3.10, 3.04, and 3.20 Å, respectively.[21]

It should be noted that the coordinates discussed above are those of protons directly adjacent the paramagnetic Yb^{3+} ion and are not necessarily identical to the coordinates of protons around Y^{3+} ions in the bulk crystal. In Sec. V a method is suggested for more accurately determining the bulk proton coordinates. Using the large magnetic moment of Tb^{3+} in YES:Tb^{3+}, well-resolved NNMR signals from several unit cells containing Y^{3+} ions are readily observed. The positions of protons in these Y^{3+} cells may be obtained from field angle dependences as described in Sec. IV D.

D. Dependence on field angle

Although the local-field components at $\theta = 0$ can be uniquely determined by a frequency dependence, more information about the form of the interaction is obtained by measuring the NNMR splittings as the angle of the external field is varied. For the general interaction $\vec{S} \cdot \vec{A} \cdot \vec{I}$, a field angle dependence of the near-nuclei splitting is necessary to determine all the components of the hyperfine tensor.[8] A knowledge of the angle-dependent splittings may allow one to empirically choose a simpler A tensor than the most general nine-parameter form. As an example, for Yb^{3+} ions situated in tetragonal sites in CaF_2, the angle dependence of the first shell fluorine splittings was found to fit a simple dipolar-plus-scalar (two parameter) interaction to within a few percent.[16] Thus even in the case of a significantly covalent interaction it was possible to derive a reasonable measure of the lattice distortion around the paramagnetic ion. In the present case, Yb^{3+} in YES, the angle dependence of the nearest protons also reveals small but significant deviations from a pure point dipolar interaction; even though the covalent contributions are much less than for CaF_2.

The experimental difficulties of an angle dependence are apparent. A large degeneracy in the spectrum occurs when H is along the symmetry axis. For example, all six A protons are equivalent at $\theta = 0$. As the field is rotated away from $\theta = 0$, the six A protons will resonate at six different values of the magnetic field (see Fig. 18). Thus at an arbitrary field angle there is a large increase in the complexity of the spectrum as well as the sensitivity needed to detect the resonances.

An angle dependence of the A proton resonances is shown in Fig. 12, along with the best fit to the point dipolar interaction, Eqs. (5) and (7). This

TABLE III. Local-field components h_z and h_ρ derived for the nearest water protons from a least-squares fit to the data of Fig. 11. Corresponding spacial coordinates (r, φ) of the protons assume a point dipolar interaction with the Yb^{3+} moment [Eqs. (9) and (10)].

Site	h_z (G)	h_ρ (G)	r (Å)	φ (deg)
A	423	879	2.95	41.14
D	−152	734	3.03	60.44
F	−393	313	3.21	76.71

was a three-parameter fit to the data of all 12 branches simultaneously. The resulting coordinates of proton A were $r = 2.94$ Å and $\varphi = 41.4°$, which compare very favorably to the values in Table III obtained from the frequency dependence. The third parameter was the azimuthal angle, determining the plane in which H was rotated.

The imperfect fit to the data is attributed to the simple interaction which was used. Some corrections to the point dipole model which have been considered are the following:

1. Scalar interaction

It was found that the addition of a scalar Fermi contact interaction of the form $A\vec{I}\cdot\vec{S}$ to the spin Hamiltonian does not significantly improve the theoretical fit to the data. This is not a surprising result since (unlike CaF_2:R) there is an oxygen atom between the impurity and the nearest nucleus, greatly reducing the probability that the electronic wave function will directly overlap the nucleus. The absence of a direct overlap is further substantiated

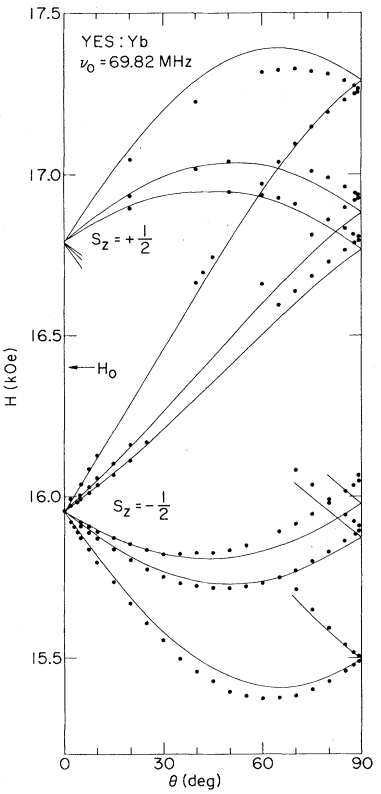

FIG. 12. Dependence of the A proton NNMR splittings as the magnetic field is rotated with respect to the crystalline axis. θ is the angle between $\vec{H}$ and the c axis. The solid curves are a single least squares fit to the data assuming the dipolar interaction of Sec. II and $g_\perp = 0$. Both $S_z = \pm\frac{1}{2}$ branches are included in the fit.

TABLE IV. Measured splittings $(H - H_0)_{exp}$ of proton F at $\theta = 0°$ for four rare-earth ions in YES. $(H - H_0)_d$ is the calculated dipolar splitting in gauss using x-ray-estimated position of proton F.

Ion	$g_\parallel$	$(H - H_0)_{exp}$	$(H - H_0)_d$	% diff.
Yb^{3+}	3.328	390	388.8	0.3
Tb^{3+}	17.72	2000	1993	0.35
Dy^{3+}	10.94	1286	1252	3.7
Nd^{3+}	3.665	427.5	428	0.1

in Sec. VI (Table IV) where data for several different rare-earth impurities are compared.

2. Higher-order Zeeman interaction

In general one must take into account admixtures of higher electronic states ($|\pm\frac{5}{2}\rangle$, $|\pm\frac{7}{2}\rangle$, $|\pm\frac{1}{2}\rangle$) into the ground doublet ($|\pm\frac{3}{2}\rangle$) via the electronic Zeeman interaction. For a given field angle these second-order admixtures will cause $\langle S_z\rangle$ to be dependent on magnetic field. However for YES:Yb^{3+} the first excited doublet is rather high (44 cm^{-1}) and the admixtures are small for $H \lesssim 20$ kOe. It was found that the second-order Zeeman correction to the NNMR splittings is less than 3 G over the given field range.

3. Higher multipole moments

In the absence of a large covalent overlap with the hydrogen atoms the finite extent of the impurity wave function may best be described by a series of multipole moments at the impurity site, with the dipole moment dominant. Since the C_{3h} site lacks inversion symmetry, a quadrupolar moment is not excluded. While this approach has not yet been examined in detail, it would possibly contribute another physically significant parameter, the quadrupolar moment, which is dependent on the electron spin-density distribution.

E. Behavior near $\theta = 90°$

A particularly interesting aspect of the YES : Yb crystal is the extreme anisotropy of the electron g factor. For a pure $J_z = \pm\frac{3}{2}$ doublet, $g_\parallel = 3.43$ and $g_\perp = g_L\langle\frac{3}{2}|J_+ + J_-|-\frac{3}{2}\rangle = 0$. The value of $g_\perp$ for Yb^{3+} may in fact differ from zero when higher electronic levels admix with the $|\pm\frac{3}{2}\rangle$ ground doublet, caused by slight local variances in the crystal-field symmetry or by higher-order Zeeman admixture. The value of $g_\perp$ is a crucial parameter in the theory of the nuclear spin refrigerator. The basic question is whether the electronic Zeeman levels actually *cross* the nuclear Zeeman levels near $\theta = 90°$. For a crossing to occur the value of $g_\perp$ must be less than the proton g factor, $g_n = 0.00304$. An exact

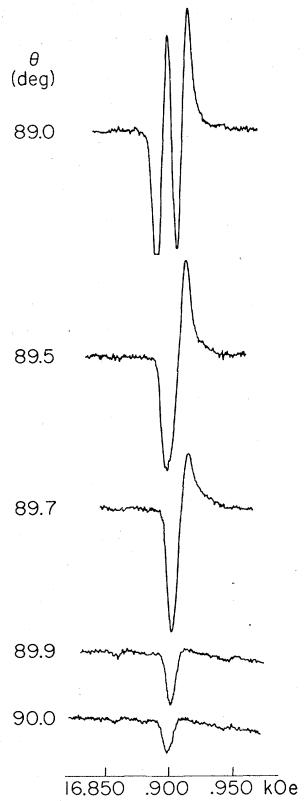

FIG. 13. Behavior of a proton A resonance as θ approaches 90°. The intensity becomes greatly reduced and the line shape is asymmetric as $\theta \to 90°$.

measure of this important parameter is difficult; however, the value $g_\perp \approx 0.01$ has been determined from the ESR intensity at $\theta = 0°$, and this value is consistent with recent spin refrigerator measurements and theory.[29,45]

The small $g_\perp$ has a striking effect on the near-proton splittings; indeed, a rather direct measure of $g_\perp$ may be obtained from these experiments. In the limiting case of $g_\perp = 0$, one finds that $\langle S_z \rangle = \pm\frac{1}{2}$ and $\langle S_x \rangle = \langle S_y \rangle = 0$ for all angles $\theta \neq 90°$. This means that, from Eq. (4), the electronic moment $\vec{\mu}_e$ is rigidly aligned along the crystalline c axis independent of the external field angle. Consequently the local dipole field, Eq. (5), is also fixed in the crystal. For small but finite $g_\perp$, one finds that $\langle S_z \rangle$, $\vec{\mu}_e$ and $\vec{h}$ become greatly reduced as θ nears 90°. The electronic moment for $\theta = 90°$ is $\epsilon = g_\perp/g_\parallel$ times that for $\theta = 0°$; thus, in this idealized case the near-proton resonances would all suddenly collapse towards the bulk resonance as $\theta \to 90°$. For a well-defined $g_\perp = 0.01$ this collapse of the near proton spectrum would occur at angles $\theta > 89°$. The observed behavior was unexpectedly quite different.

Figure 13 shows what actually happens for the proton A resonance when θ approaches 90°. Two branches (corresponding to two nonequivalent A protons) coalesce near 89.5°, as in Fig. 12; however, the remaining single resonance does not shift towards H_0 as suggested above. At larger angles the resonance changes shape and becomes much smaller in intensity. But no obvious collapse towards H_0 occurs. Indeed a finite unshifted signal still remains at $\theta = 90°$. This fact can be verified by setting the field on resonance and rotating slowly through the $\theta = 90°$ plane—the signal never vanishes.

This behavior is characteristic of a smooth distribution of $g_\perp$ values and not of a single well defined $g_\perp$. The finite unshifted signal at $\theta = 90°$ is consistent with this model if one takes into account a small "c axis wander" characteristic of this type of crystal. To describe this phenomenon we observe that the ground-state wave function for the electron spin-$\frac{1}{2}$ Hamiltonian is

$$|a\rangle = 2^{-1/2}\left[\left(1+\frac{g_\parallel \cos\theta}{g}\right)^{1/2}\left|-\tfrac{1}{2}\right\rangle + \left(1-\frac{g_\parallel \cos\theta}{g}\right)^{1/2}\left|\tfrac{1}{2}\right\rangle\right], \tag{25}$$

which gives the expectation value of S along the c axis,

$$\langle S_z \rangle = \langle a | S_z | a \rangle = \tfrac{1}{2}(1+\epsilon^2 \tan^2\theta)^{-1/2}. \tag{26}$$

For $\epsilon \tan\theta \ll 1$, the near-proton splitting is proportional to $\langle S_z \rangle$, and $\langle S_z \rangle \approx \frac{1}{2} - \frac{1}{4}\epsilon^2 \tan^2\theta$, with $\epsilon = g_\perp/g_\parallel$.

We consider a Gaussian distribution of $g_\perp$ values throughout the crystal, $\exp(-g_\perp^2/2\sigma)$, where $\sigma^{1/2} = \bar{g}_\perp$ is the rms deviation about $g_\perp = 0$. We wish to calculate the number $N(\theta)$ of impurity sites contributing to the near-proton resonance when the field angle is θ. Thus we sum over all sites where $g_\perp$ is not large enough to shift the local NNMR resonance by more than the nuclear linewidth ($\Delta H \approx 5$ G). Those sites with $g_\perp$ greater than this $g_\perp'(\theta)$ will not contribute to the intensity of the observed resonance, Fig. 13. For proton A the splitting $h_\perp$ at 89° is 500 G, so the criterion $2(\langle S_z \rangle - \frac{1}{2}) = \Delta H/h_\perp$ gives $g_\perp'(\theta) = (2\Delta H/h_\perp)^{1/2} g_\parallel/\tan\theta = 0.47/\tan\theta$. Thus at a given field angle θ the number of impurity sites contributing to the near-proton resonance is

$$N(\theta) = \frac{N_0}{(2\pi\sigma)^{1/2}} \int_0^{g_\perp'(\theta)} \exp\left(\frac{-g_\perp^2}{2\sigma}\right) dg_\perp, \tag{27}$$

where N_0 is the total number of impurity sites in the crystal. This expression has been calculated numerically over the angles of interest for several values of $\bar{g}_\perp$ and is compared in Fig. 14 to the measured A proton intensities. A reasonable fit to the data is obtained for $\bar{g}_\perp = 0.01$, which is remarkably close to the value of $g_\perp$ determined from the ESR intensity.

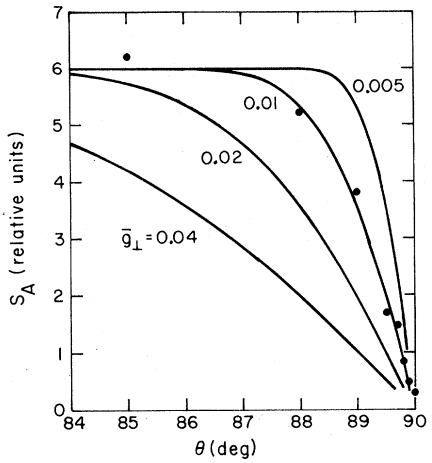

FIG. 14. Dependence of the NNMR intensity near $\theta = 90°$ for YES:Yb, from the data of Fig. 13. The solid curves, Eq. (27), assume a Gaussian distribution of $g_\perp$ throughout the crystal with an rms deviation $\bar{g}_\perp$ about $g_\perp = 0$.

The remaining signal at 90° is explained by considering a small angular distribution in the c axis throughout the crystal, as has been observed previously.[24] The angular deviation needed to explain the observed intensity is $\delta\theta_{\rm rms} \approx 0.2°$ for this large heavily doped crystal, Yb 1.

The change in derivative line shape, Fig. 13, also appears to be consistent with this interpretation. The power absorbed approaches a step function as $\theta \to 90°$, showing that the protons are resonating over a range of fields between $H_0 - h_\perp$ and H_0 depending upon the local $g_\perp$ at a given impurity site.

The new result here is that there exists a large quasicontinuous distribution of $g_\perp$ values throughout the crystal. The rms deviation $\bar{g}_\perp \approx 0.01$ is about three times the proton g factor; however, there are significant numbers of sites with $g_\perp$ both larger and smaller than this average value.

F. In search of hidden $S_z = +\frac{1}{2}$ resonances

Half of the near-proton spectrum is comprised of $S_z = +\frac{1}{2}$ "mirror" resonances which are weaker than the principal $S_z = -\frac{1}{2}$ resonances by the electronic Boltzmann factor, and they are often obscured by the latter. For YES:Yb, a prime example is the A mirror line occurring somewhere under the F principal lines. To remedy this situation a double-frequency experiment has been devised which precisely determines the position of this obscured mirror resonance: while the intensity of the principal A resonance is monitored as usual with $H = 15.920$ kG at $\nu_0 = 69.703$ MHz, a second high-level rf signal at frequency ν_1 is applied to the crossed coil through an external matching circuit (see Fig. 5 caption). The purpose of the second-signal generator is to saturate the polarization p_A of proton A at its $S_z = +\frac{1}{2}$ resonance, while p_A is observed at the $S_z = -\frac{1}{2}$ resonance. The result is shown in Fig. 15. Here, the frequency ν_1 is continuously swept by applying a slowly varying dc ramp voltage to the FM input of the second rf generator. When ν_1 corresponds to the resonance frequency of the A mirror line, a dip is observed in the intensity of the *principal* A line. The reason for the reduced A polarization is simply that the A proton spin is being partially saturated when $S_z = +\frac{1}{2}$, and its polarization remains reduced when the electron flips to $S_z = -\frac{1}{2}$. In this experiment, saturation of the F resonances has no effect on the A polarization; thus, only the A mirror resonance appears in the ν_1 frequency sweep. The frequency scale of Fig. 15(b) is aligned with the field sweep of Fig. 15(a) for $\nu_0 = 69.703$ MHz by the approximate relation $\nu_1 - \nu_0 = (g_n \mu_B/h)(15\,920 - H)$. The resulting position of the A mirror resonance is clearly consistent with the field sweep of Fig. 15(a), which shows a hint of a small derivative resonance at the same position.

A similar experiment has been performed for the completely resolved resonances of the F proton site with an amusing result, shown in Fig. 16. As expected, it is found that a saturation of the $F1$ mirror causes a reduction of the $F1$ principal line; however, saturation of the $F2$ mirror can actually cause the $F1$ signal to *increase*. This is a trans-

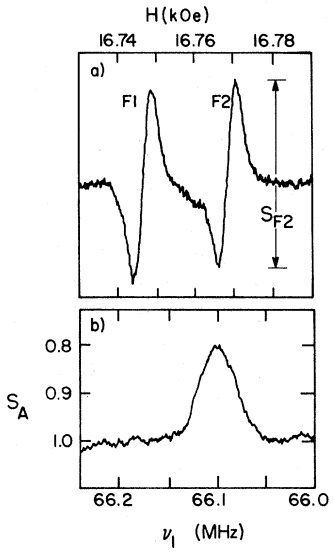

FIG. 15. (a) Usual $S_z = -\frac{1}{2}$ near-proton resonance for F protons with $\nu_0 = 69.703$ MHz and $T = 2.1$ K. The $S_z = +\frac{1}{2}$ A proton resonance occurs under these stronger F resonances and is reduced in intensity by the electronic Boltzmann ratio. (b) Double-frequency experiment showing the position of the A mirror resonance under the F principal resonances.

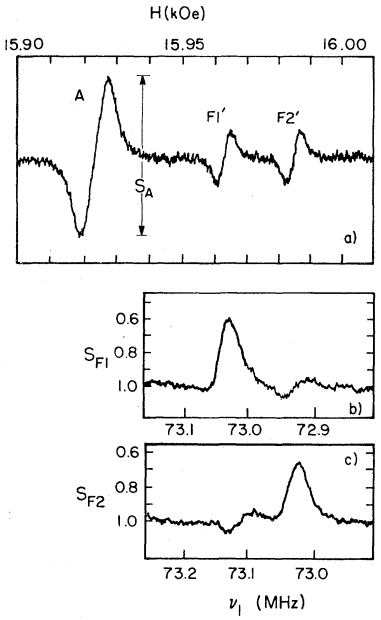

FIG. 16. (a) Magnetic field sweep over the principal A resonance and mirror F resonances at $T=2.1$ K and $\nu_0=69.703$ MHz. (b) Reduction observed in the principal $F1$ intensity as ν_1 is swept through the $S_z=+\frac{1}{2}$ resonant frequencies. $H=16.745$ kOe. (c) Reduction observed in the principal $F2$ intensity as ν_1 is swept through the $S_z=+\frac{1}{2}$ resonant frequencies. $H=16.767$ kOe. The ν_1 frequency scales are shifted to coincide with the field sweep (a) as discussed in the text.

ient effect which can be explained in terms of the dynamics of a Pake doublet, which will be discussed in a subsequent paper on relaxation of near nuclei. Basically, the two equivalent F spins belonging to one water molecule must be described in terms of the triplet spin states $|++\rangle$, $2^{-1/2}(|+-\rangle - |-+\rangle)$, and $|--\rangle$ with populations n_+, n_0, and n_-. rf saturation of one of the allowed triplet transitions, e.g., $n_- - n_0 = 0$, can result in a temporary increase in $n_+ - n_-$. Aside from this transient phenomenon, the important conclusion here is that the positions of the mirror resonances obtained by this double-frequency method are in good agreement with the directly observed spectrum of Fig. 16(a).

The double-frequency arrangement described above has also been employed to determine the thermal contact between individual near protons. Thus, by saturating one resonance and observing another, one can determine the dynamic spin-spin coupling between the two sites.

V. NEAR-PROTON SPECTRUM FOR YES: Tb^{3+}

A convenient property of the ethyl sulfate crystal is that it accepts all trivalent rare-earth ions into the Y^{3+} site of Fig. 1. The near-proton spectrum therefore is a tool which may uncover subtle differences in the local crystal structure from one impurity to the next. This sort of information may eventually lead to a more exact description of the crystal field at the impurity ion. Also, the near-proton splittings contain information about the electronic levels of the impurity which may not be directly obtainable from ESR, as for the case of Yb^{3+} near $\theta=90°$.

Since the local ethyl sulfate environment is similar for all trivalent ions, the gross features of the near-proton spectrum are expected to remain unchanged for different ions although the splittings will be scaled according to the electronic g factor. A rather spectacular spectrum has been obtained for YES doped with Tb^{3+}. This is a non-Kramers ion ($4f^8$ configuration; $^7F_6$ ground multiplet) with $g_{\parallel}=17.72$ measured by ESR for the ground doublet, indicating predominantly a $|\pm 6\rangle$ state, since $2g_L\langle +6|J_z|+6\rangle = 18$. The 100% abundant ^{159}Tb nucleus has spin-$\frac{3}{2}$, and the effective electronic spin Hamiltonian has been written

$$H=(g_{\parallel}H\cos\theta + A_{\parallel}m)S_z + \Delta_x S_x + \Delta_y S_y, \qquad (28)$$

where $A_{\parallel}=0.209$ cm^{-1}, m is the I_z quantum number of the terbium nucleus, and $\Delta^2=(\Delta_x^2+\Delta_y^2)^{1/2}=0.387$ cm^{-1} is the zero-field-splitting parameter. For all non-Kramers ions $g_{\perp}$ equals zero.

The near-proton spectrum is traced in Fig. 17 for $\vec{H}\|\vec{c}$ axis. The splitting of the low-field A resonance is 2.94 kG, and yet the linewidth remains sharp—less than 10 G. The concentration of this near-perfect 840-mg crystal (Tb 1) is estimated to be 0.5% from the near-proton intensities. Figure

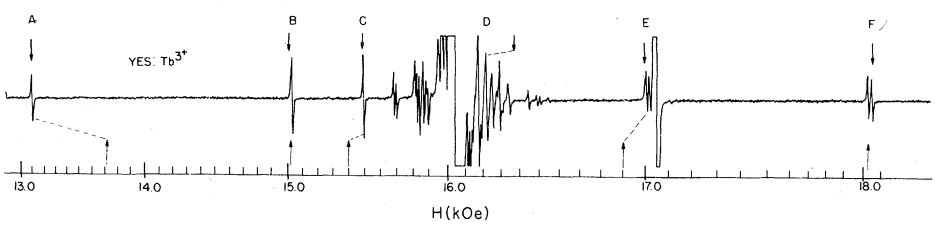

FIG. 17. Near-proton spectrum for YES:Tb^{3+}. The magnetic field is aligned accurately along the crystal c axis. $\nu_0=68$ MHz and $T=1.65$ K. The bulk resonance at 16.04 kOe is 300× off scale. The large resonance at 17.05 kOe is due to ^{19}F spins in the sample holder.

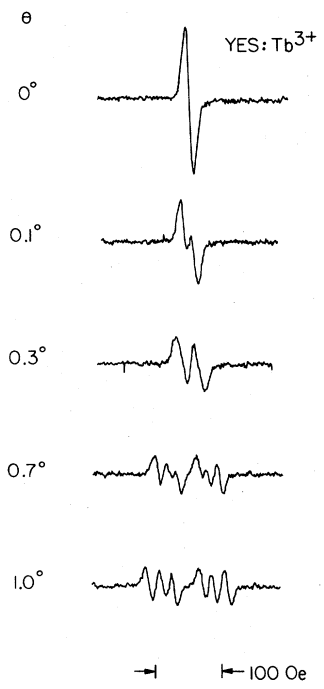

FIG. 18. Angle dependence of the A resonance in YES:Tb as H is rotated slightly away from $\theta = 0$. The six A protons (Fig. 1) are equivalent only when H is along the c axis.

18 shows the critical-field alignment necessary to obtain the sixfold degeneracy of the A protons for $\theta = 0$. A few hundredths of a degree misalignment is readily observable in this crystal.

The solid arrows above the trace in Fig. 17 are the predicted resonance positions obtained by scaling the local field components measured for Yb^{3+}. The scaling factor is the ratio of the electronic g-factors, $17.72/3.329 = 5.325$. The correspondence with the measured positions for Tb^{3+} supports the hypothesis of small covalent overlap of the unpaired spin with the hydrogen atoms, since covalency effects generally differ widely for ions having different ground wave functions (e.g., in CaF_2).[7-10]

The lower set of arrows are the predicted resonant fields using McColl's proton positions, based on the x-ray data for the oxygen positions and chemical arguments, and assuming a classical point dipolar field with $g_{\parallel} = 17.72$. Again, the F resonance is well predicted, since the known symmetry of the site fixes the positions of the F protons. For a given frequency, the quadratic shift is much larger than for Yb^{3+}. Thus, the D resonance, with $h_\rho \approx 5$ kG, occurs relatively closer to the bulk resonance.

The dependence of the A and D splittings on field angle is shown in Fig. 19. The heavy lines represent a best fit of the A resonance to the classical point dipolar form for $\theta < 80°$. The agreement is clearly better than for Yb^{3+}, probably because the unobserved $S_z = +\frac{1}{2}$ resonances are not included in the fit. Due to the extremely small Boltzmann factor, $\exp(-g_{\parallel}\mu_B H \cos\theta/kT) = 7.3 \times 10^{-5}$ at 2.0 K, $\theta = 0$, and 16.0 kG, the mirror resonances are not observed except at large field angles. The resulting A proton coordinates from this angle dependence are $r = 3.02$ Å and $\varphi = 39.62°$.

Due to the presence of the zero-field-splitting terms $\Delta_x S_x + \Delta_y S_y$ for this non-Kramers ion, the impurity moment will not remain quantized along the c axis as θ approaches 90°, even though $g_{\perp} = 0$. Thus the near-proton splittings are found to collapse for $\theta > 88°$ and no discrete resonances are observed at $\theta = 90°$. Interestingly, the hyperfine term in Eq. (28) also makes its presence known at large angles. It is found that, for $\theta > 86°$, each of the near proton resonances, which derive from only *one* proton in the unit cell, splits into four resonances, as shown in Fig. 19, corresponding to the four m values of the Tb nucleus.

The large terbium g factor results in well-re-

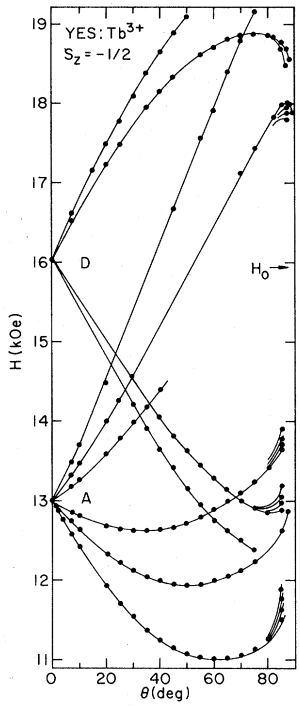

FIG. 19. Field-angle dependence of the A and D proton splittings. The solid curves through the A resonances represent a single least-squares fit to a point dipole interaction. The solid curves through the D resonances are simply smooth curves connecting the data. (Two branches were obscured by many other NNMR near H_0.) Each NNMR splits into four lines above $\theta = 86$, where the hyperfine and zero field splitting terms become important, Eq. (28).

solved near-proton splittings even for protons in adjacent unit cells. Thus YES:Tb^{3+} appears to be an excellent crystal for determining the precise positions of the protons in adjacent Y^{3+} cells via field angle dependence. This information may be useful for example in calculating the nuclear diffusion constant for pure YES.[46]

VI. CONCLUSIONS

In addition to the Yb^{3+} and Tb^{3+} experiments just described, near-proton spectra have been observed for Dy^{3+} and Nd^{3+} in YES. An informative comparison of the F proton splitting near each of these ions is given in Table IV. In all four cases the measured splitting is close to the predicted splitting obtained from a point dipolar field with the appropriate g factor as measured from ESR. These data again indicate that the covalent overlap of the rare-earth ion onto the proton site is small. By comparison, for cubic rare-earth sites in CaF_2 the covalent contribution to A_p varies widely in magnitude and sign depending upon the particular paramagnetic impurity.[2,7-10]

The principal objective of this paper was to determine the effects on the near-proton resonances of all the experimental parameters: impurity concentration, NMR frequency, temperature, and magnetic field angle. For YES : Yb^{3+} well resolved spectra were observed at rather large impurity concentrations, 0.2%–5% and 2%, respectively. For these two cases, mutual electronic spin flips between impurities is suppressed by the small $g_\perp$ factors. Thus, as expected, no lifetime broadening of the NNMR's due to mutual electronic spin flips was observed. For YES:Yb, a temperature dependent broadening of the near-proton resonances was observed above $T = 3.8$ K which was explained by rapid electronic spin-lattice relaxation. The resulting reduction in NMR derivative intensity with temperature gave a numerical estimate of the coefficient for the Orbach relaxation process: $(1.6 \pm 0.3) \times 10^{12} \exp(-63/T)$ $(\sec^{-1})$. A broadening of the NNMR resonances occurs when the correlation time τ associated with $\langle S_z \rangle$ becomes less than about 10^{-5} sec.

Frequency dependences of the YES:Yb NNMR splittings at $\theta = 0$ were observed between 20 and 80 MHz for the nearest protons. These data gave the components of the local field at particular proton sites, from which an estimate of the proton positions was obtained. Field angle dependence of the near proton splittings indicate the need for a refinement of the simple dipole field. The observed deviations contain information about the finite extent of the impurity wave functions.

An important aim of this paper was to define the experimental parameters necessary to observe near-nuclei resonances in crystals. The conclusion is that this high-sensitivity NMR technique is applicable to a wide variety of paramagnetic crystals at low temperatures. These studies also reveal the broad range of experimental conditions under which near-nuclei magnetic resonance may be observed. This type of experiment can be a useful method for studying electron-nuclear spin interactions in a variety of paramagnetic crystals.

ACKNOWLEDGMENTS

I am deeply grateful to Professor C. D. Jeffries for supporting this work and for many enjoyable years under his selfless tutorage. A. R. King provided the impetus for these experiments by proving that detection of near-protons in thermal equilibrium was indeed possible. His patience and experimental finesse inspired this work. R. L. Ballard provided valuable ideas in the early stages of these experiments. I wish to thank R. S. Markiewicz for assisting in computer fitting of the field angle dependences. Analysis of these experiments was completed at the Physics Department and Materials Research Laboratory of the University of Illinois at Urbana-Champaign. I thank C. P. Slichter for his useful comments.

*Supported in part by the U.S. Energy Research and Development Agency Contract No. E(04-3)-34, Project 20 (Berkeley) and NSF Grant No. DMR-76-01058 (Ill.).

†Present address: Physics Dept., University of Illinois, Urbana, Ill. 61801.

[1]See for example, A. Abragam and B. Bleaney, *Electron Paramagnetic Resonance of Transition Ions* (Clarendon, Oxford, 1970), and references cited therein.

[2]J. M. Baker and J. P. Hurrell, Proc. Phys. Soc. Lond. 82, 742 (1963).

[3]For rare-earth ions the electron-nuclear interaction is generally too small to result in resolved superhyperfine structure. Some exceptions are reported by J. M. Baker, W. Hayes and M. C. M. O'Brien, Proc. Soc. A 254, 273 (1960); F. K. Naehring, Phys. Status Solidi B 55, 247 (1973).

[4]G. Feher, Phys. Rev. 103, 500 (1956); 114, 1219 (1959).

[5]Al_2O_3: N. Lawrance, E. C. McIrvine and J. Lambe, J. Phys. Chem. Solids 23, 515 (1962); J. Lambe, N. Lawrance, E. C. McIrvine, R. W. Terhune, Phys. Rev. 122, 1161 (1961).

[6]Alkali halides: H. Seidel, Z. Phys. 165, 218 (1961); L. F. Mollenauer, S. Pan, and A. Winnacker, Phys. Rev. Lett. 26, 1643 (1971).

[7]CaF_2: U. Ranon and James S. Hyde, Phys. Rev. 141, 259 (1966).

[8]CaF_2: J. M. Baker, E. R. Davies, and J. P. Hurrell, Proc. R. Soc. A 308, 403 (1968); D. Kiro and W. Low, in *Magnetic Resonance*, edited by C. K. Coogan, N. S. Ham, S. N. Stuart, J. R. Pilbrow, and G. V. H. Wilson

(Plenum, New York, 1970); H. Bill, Phys. Lett. A29, 593 (1969); W. Kolbe and N. Edelstein, Phys. Rev. B 4, 2869 (1971).

[9] KH_2AsO_4: N. S. Dalal and C. A. McDowell, Phys. Rev. B 5, 1074 (1972); myoglobin: C. P. Scholes, R. A. Isaacson, and G. Feher, Biochim. Biophys. Acta 263, 448 (1972).

[10] R. de Beer, thesis (Delft, 1971) (unpublished).

[11] The initial experiments were reported by A. R. King, J. P. Wolfe, and R. L. Ballard, Phys. Rev. Lett. 28, 1099 (1972).

[12] N. Bloembergen, Physica (Utr.) 16, 95 (1950).

[13] R. Shulman and V. Jaccarino, Phys. Rev. 107, 1196 (1957).

[14] D. V. Lang, J. B. Boyce, D. C. Lo, and C. P. Slichter, Phys. Rev. Lett. 29, 776 (1972); J. B. Boyce and C. P. Slichter, Phys. Rev. B 13, 379 (1976).

[15] To date no ENDOR spectrum has been reported for a non-Kramers ion. Non-Kramers ions (an even number of unpaired electrons) typically display electric-dipole transitions, $g_\perp = 0$, rapid spin-lattice relaxation, and large zero-field splittings sensitive to crystal strains. Observation of ESR is often difficult (e.g., in CaF_2). The NNMR experiments, on the other hand, do not require detection and saturation of the ESR.

[16] J. P. Wolfe and R. S. Markiewicz, Phys. Rev. Lett. 30, 1105 (1973).

[17] J. P. Wolfe, Phys. Rev. Lett. 31, 907 (1973).

[18] G. H. Dieke, *Spectra and Energy Levels of Rare Earth Ions in Crystals* (Interscience, New York, 1968).

[19] J. A. A. Ketelaar, Physica (Utr.) 4, 619 (1938).

[20] D. R. Fitzwater and R. L. Rundle, Z. Kristallogr. 112, 362 (1959).

[21] J. R. McColl and C. D. Jeffries, Phys. Rev. B 1, 2917 (1970). J. R. McColl, thesis (Univ. of California-Berkeley, 1968) (unpublished).

[22] R. G. Wheeler, F. M. Reames, and E. J. Watchel, J. Appl. Phys. 39, 915 (1968).

[23] E. Y. Wong, J. Chem. Phys. 39, 2781 (1963).

[24] J. P. Wolfe and C. D. Jeffries, Phys. Rev. B 4, 731 (1971).

[25] M. Berti, L. Cianchi, M. Mancini, and G. Spina, Phys. Lett. A 40, 263 (1972). See also, M. Inoue, Phys. Rev. Lett. 11, 196 (1963); R. J. Birgeneau, *ibid.* 19, 160 (1967).

[26] K. H. Langley and C. D. Jeffries, Phys. Rev. 152, 358 (1966).

[27] H. B. Brom and W. J. Huiskamp, Physica (Utr.) 60, 163 (1972).

[28] W. H. Potter and H. J. Stapleton, Phys. Rev. B 5, 1729 (1972).

[29] R. L. Ballard, thesis (University of California-Berkeley, 1971) (unpublished).

[30] J. P. Wolfe, Chem. Phys. Lett. 37, 256 (1976).

[31] J. P. Wolfe and A. R. King, Chem. Phys. Lett. 40, 451 (1976).

[32] E. E. Hundt, H. H. Niebuhi, B. Derighett, and E. Brun, *Proceedings of the Fifteenth Congress AMPERE* (1970) (North-Holland, Amsterdam, 1970); E. E. Hundt, thesis (Universität Zürich, 1972) (unpublished).

[33] The use of an rf hybrid tee and broadband mixer detection for NMR was originally proposed by M. P. Klein and D. E. Phelps, Rev. Sci. Instrum. 38, 1545 (1967). An early version of the spectrometer used in our laboratory and developed in collaboration with A. R. King is described in J. P. Wolfe, First Latin American Symposium on Magnetic Resonance, Lima, Peru, 1973 (unpublished).

[34] C. P. Poole, *Electron Spin Resonance* (Interscience, New York, 1967), Chap. 6.

[35] H. J. Stapleton (private communication); M. D. Kemple, thesis (University of Illinois at Urbana, 1971), p. 138 (unpublished).

[36] A different method is used by E. H. Erath, J. Chem. Phys. 34, 1985 (1961).

[37] G. E. Pake, J. Chem. Phys. 16, 327 (1948).

[38] W. S. Benedict, N. Gailer, and E. K. Plyler, J. Chem. Phys. 24, 1139 (1956).

[39] This point is academic for YES:Yb where the interaction is mostly point dipolar; but, for Yb^{3+} in CaF_2 the first-shell ^{19}F interaction is largely covalent and the sign of the interaction is not known *a priori*. It is not usually possible to identify the sign of S_z for ENDOR resonances since the intensities of the transitions depend upon complicated relaxation processes. See also, J. M. Baker and W. B. J. Blake, Phys. Lett. A 31, 61 (1970); and Ref. 16.

[40] J. Van den Broek and L. C. Van der Marel, Physica (Utr.) 30, 565 (1964).

[41] Other linewidth broadening mechanisms for near nuclei include local strains, c-axis wander, and random fields of nearby impurities.

[42] See, for example, Ref. 34, Chap. 20 and p. 799.

[43] This analysis applies only to well resolved near-nuclei resonances. No linewidth broadening will occur for distant nuclei where the nuclear-nuclear interaction $\hbar\Delta\omega$ is larger than the electron-nuclear interaction $g_n\mu_B h_z$.

[44] L. L. Buishvili, G. R. Khutsishvili, and M. D. Zviadadze, Phys. Status Solidi B 48, 851 (1971).

[45] H. B. Brom, Phys. Lett. A 41, 73 (1972).

[46] J. V. Gates and W. H. Potter, Phys. Rev. B 13, 8 (1976).